OPTICAL MAPPING OF INTRAMURAL WAVE PROPAGATION

Arkady Pertsov

SUNY Upstate Medical University

Experimental evidence

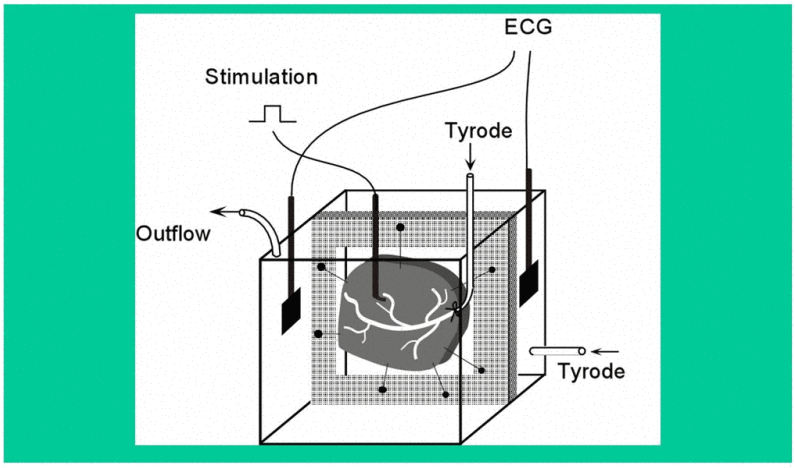

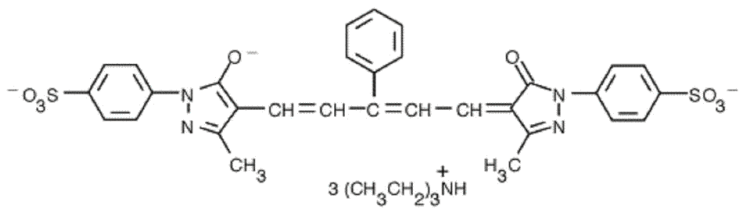

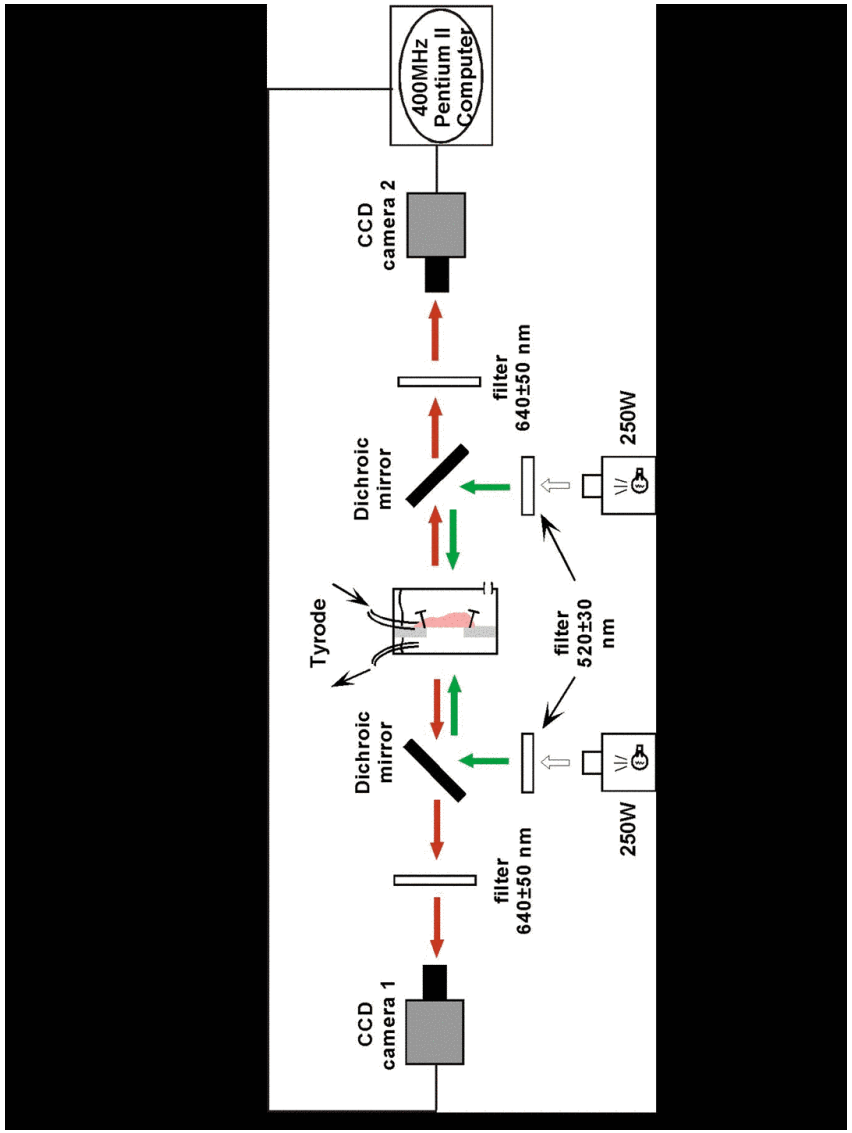
400MHz Pentium II Computer
CCD camera 2
filter 640±50 nm
Dichroic mirror
250W
Tyrode
filter 520±30 nm
Dichroic mirror
250W
filter 640±50 nm
CCD camera 1

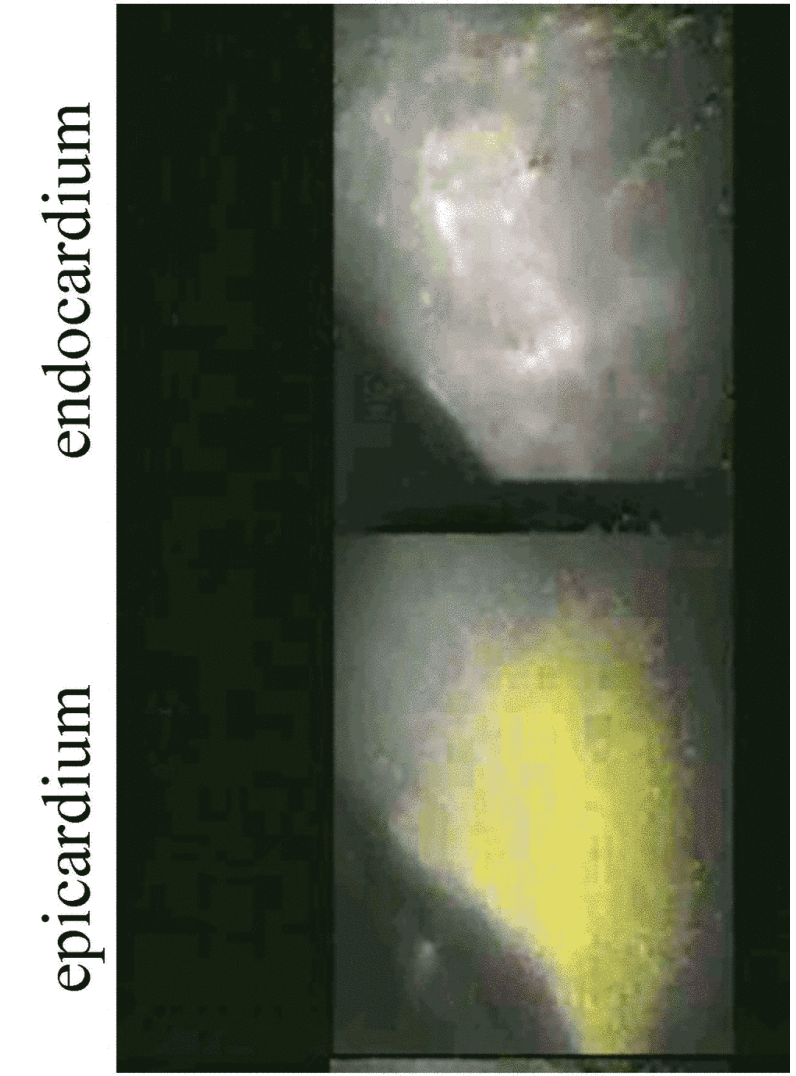
epicardium
endocardium

epicardium endocardium

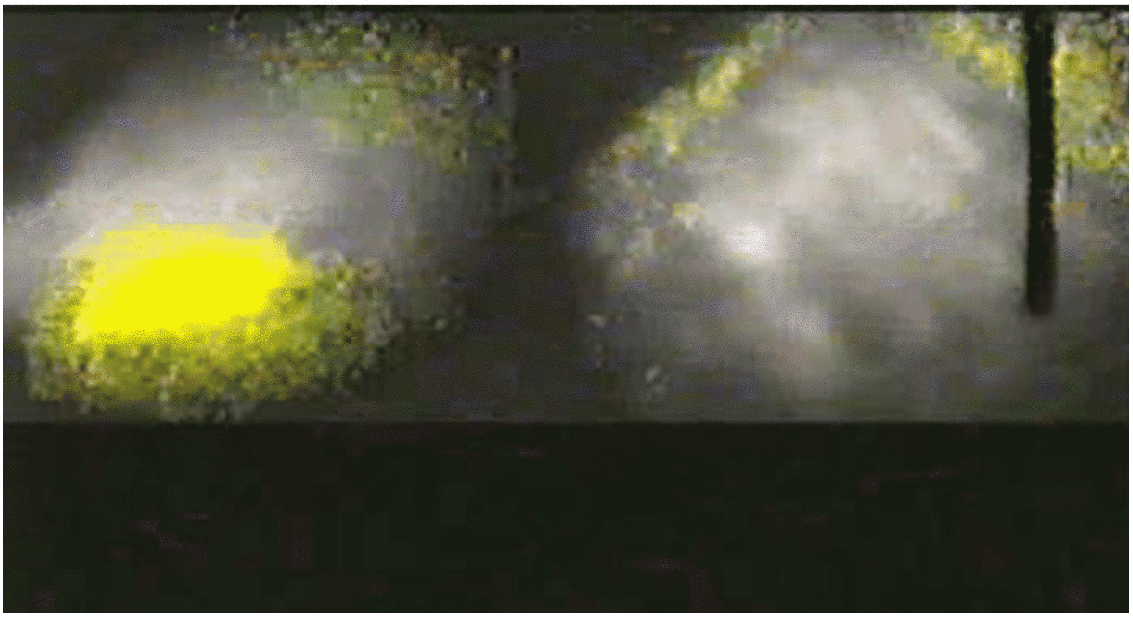

L-shaped filament

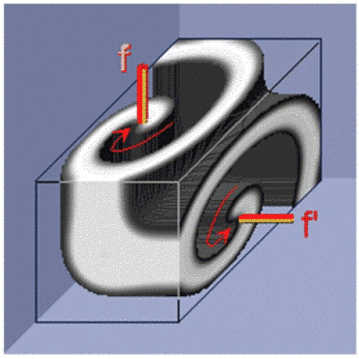

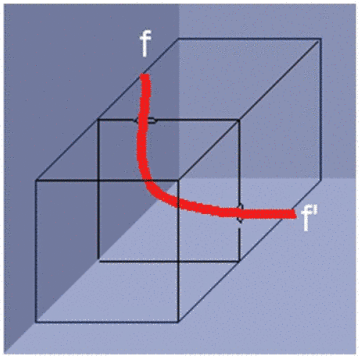

Optical Mapping Methods

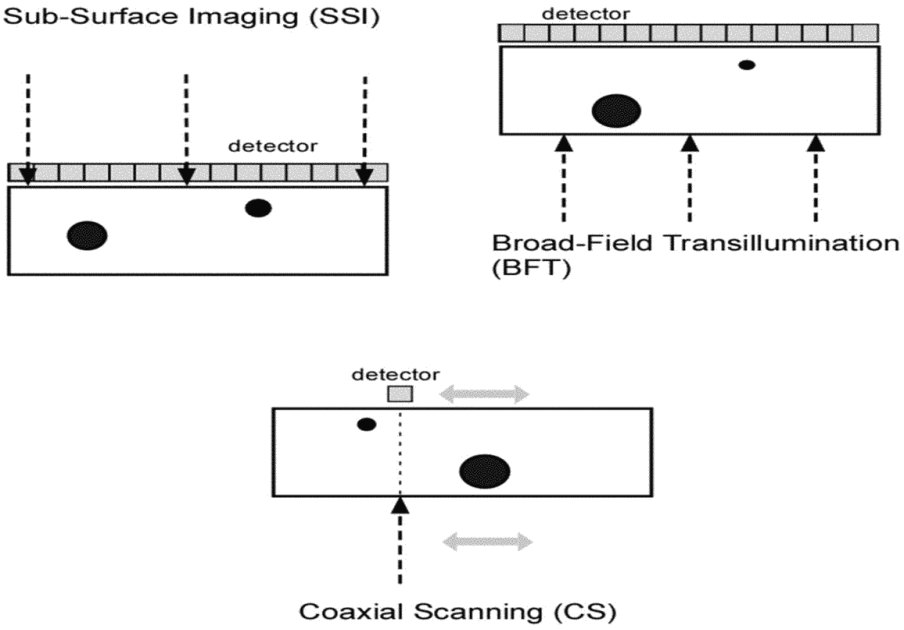

Hybrid model

Light absorption and scattering + Action potential propagation = Voltage-dependent Optical signal

$$D\nabla^2\Phi(\vec{r}) - \mu_a\Phi(\vec{r}) + Q(\vec{r}) = 0$$

$$Q(\vec{r}) \sim \beta \cdot V_m(\vec{r}) \cdot \Phi_e(\vec{r})$$

Calculating the PSF in a slab of thickness L (1)

- Analytical solution based on Dirichlet boundary conditions:

$$psf(R,z') = \frac{1}{2\pi}\int_0^\infty \frac{\xi J_0(\xi R)\sinh\eta(L-z')}{\sinh\eta L}d\xi$$

$$\eta = \sqrt{\xi^2 + (\frac{\mu_a}{D})^2}$$

- Computationally efficient approximation based on hyperbolic functions

Calculating PSF in a slab of thickness L (2)

Solution based on the **method of images** allows for use of different boundary conditions (Dirichlet, Robin, …).

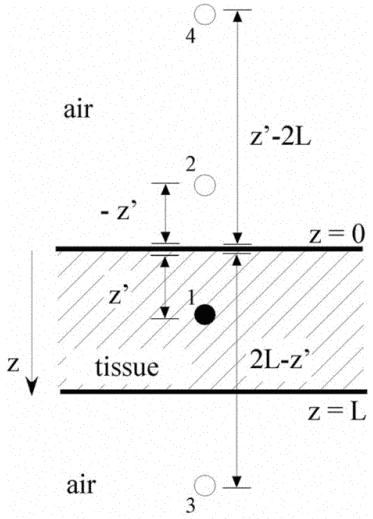

slab geometry

3D-information from the conventional epi-fluorescence mapping

$$\frac{\Delta F}{F} \sim \Delta V_m$$

$$\frac{\Delta F}{F} \sim \int_V \Delta V_m dV$$

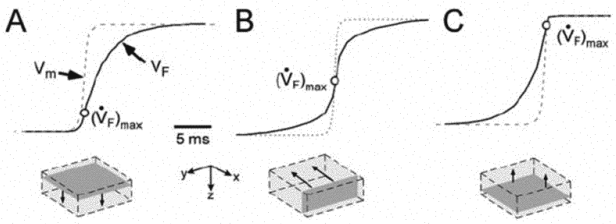

FIGURE 4 OAP upstroke morphology as a function of the direction of transmural propagation (see diagrams below each plot). (*A*) Propagation away from the recording surface; (*B*) propagation perpendicular to the recording surface; and (*C*) propagation toward the recording surface. Open circles on the OAP upstrokes indicate (the Fenton-Karma ionic model) locations of $(\dot{V}_F)_{max}$. Electrical upstrokes are indicated by dashed lines.

Biophysical Journal 85(4) 2673–2683

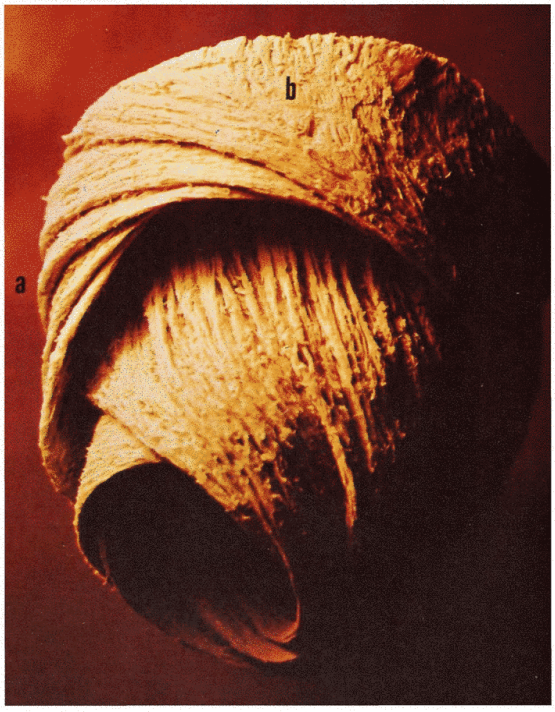

Torrent-Guasp F. The cardiac muscle. Juan March Foundation. 1973.

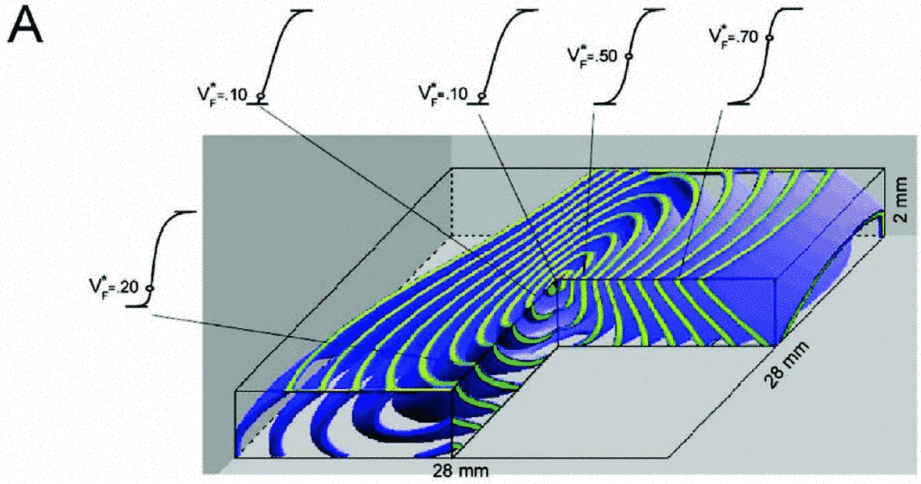

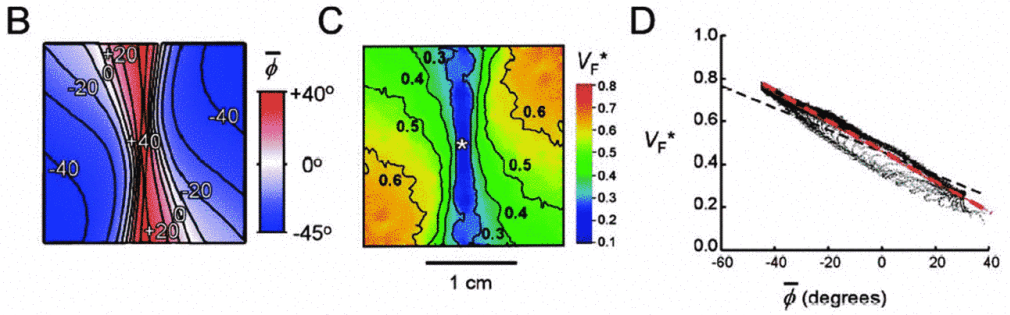

Figure 3. Subsurface wavefront orientation and spatial variation in OAP upstroke morphology after epicardial point stimulation. A, Simulated epicardial and transmural (cutaway) isochrone maps (interval, 5 ms). The corresponding OAP upstrokes at 5 different sites are shown (left and top). Open circles on the OAP upstrokes indicate the location of V_F^*. B, Map of the optically weighted mean angle, $\bar{\phi}$, for this simulation (isolines of $\bar{\phi}$ are indicated). C, Corresponding V_F^* map, with isolines of V_F^* indicated. D, Plots showing the relationship between V_F^* vs $\bar{\phi}$ at all corresponding pixels in the $\bar{\phi}$ and V_F^* maps in B and C, respectively. The thick dashed red line is the linear regression of V_F^* vs $\bar{\phi}$. For comparison, the thin black dashed line shows the linear regression of V_F^* vs $\bar{\phi}$ for steady-state waves fronts (from Figure 1C).

Guinea pig LV

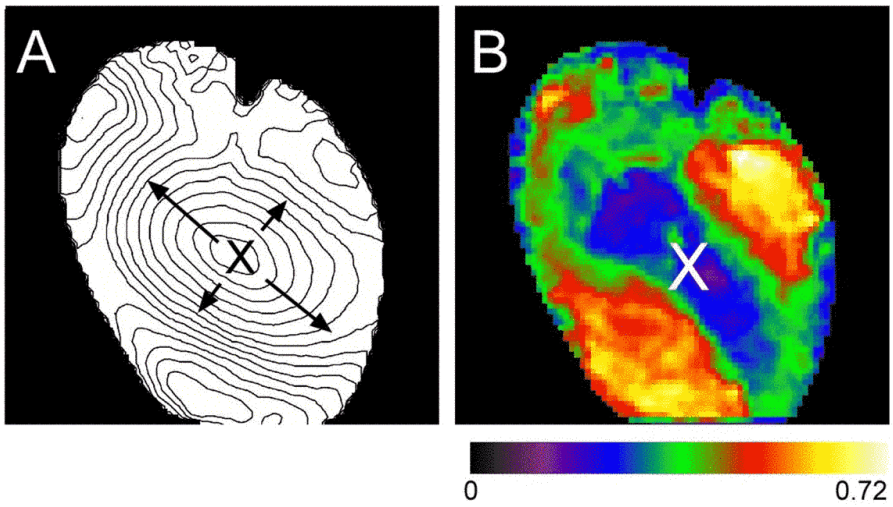

Transillumination

extracting information from
deep inside myocardial wall

visualization of scroll wave filaments

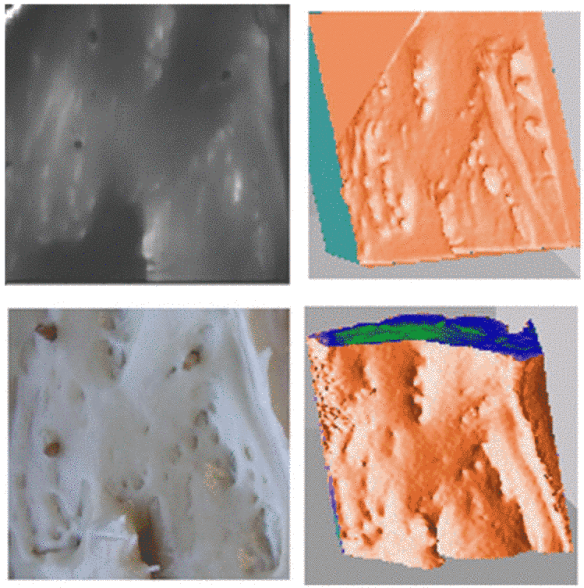

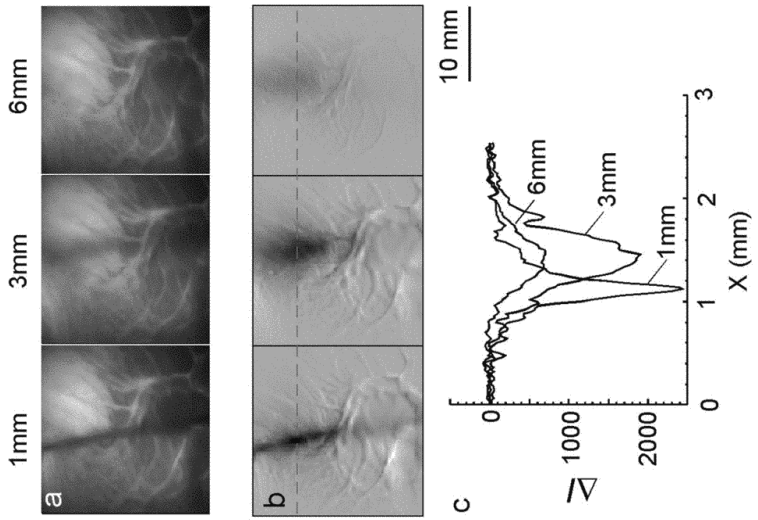
6mm
3mm
1mm
a
b
c
10 mm
6mm
3mm
1mm
0
1000
2000
/∇/
0
1
2
3
X (mm)

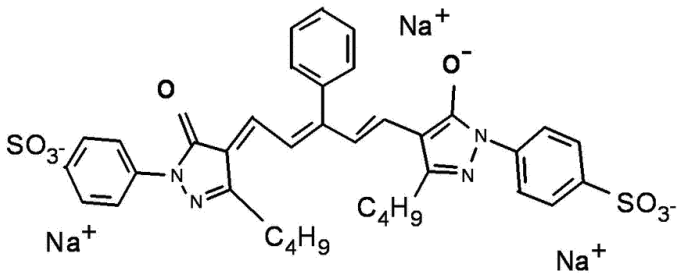

Absorption voltage-sensitive dye JPW 1150.

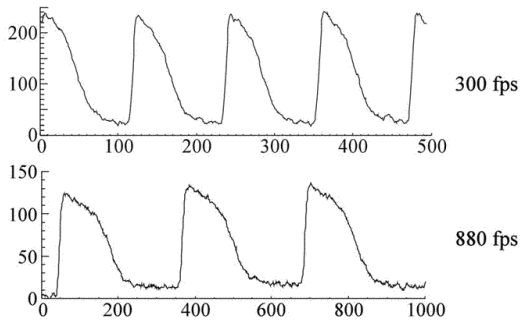

Transillumination signals obtained using JPW 1150

NATURE | VOL 386 | 3 APRIL 1997

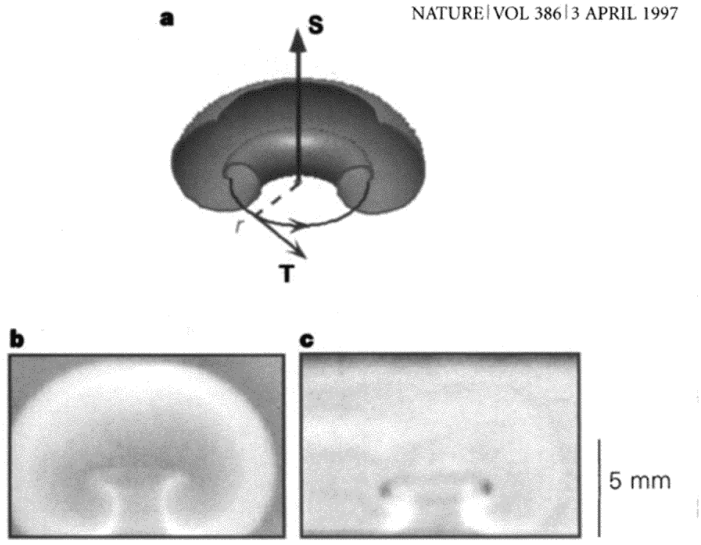

Figure 1 a, Schematic cross-section of a scroll ring. The dark circle of radius *r* in the centre is the filament of the ring, about which the wave rotates (the spiral on the right rotates clockwise). The unit tangent vector **T** is in the direction of the local

Michael Vinson*†, Sergey Mironov*‡, Scott Mulvey* & Arkady Pertsov*

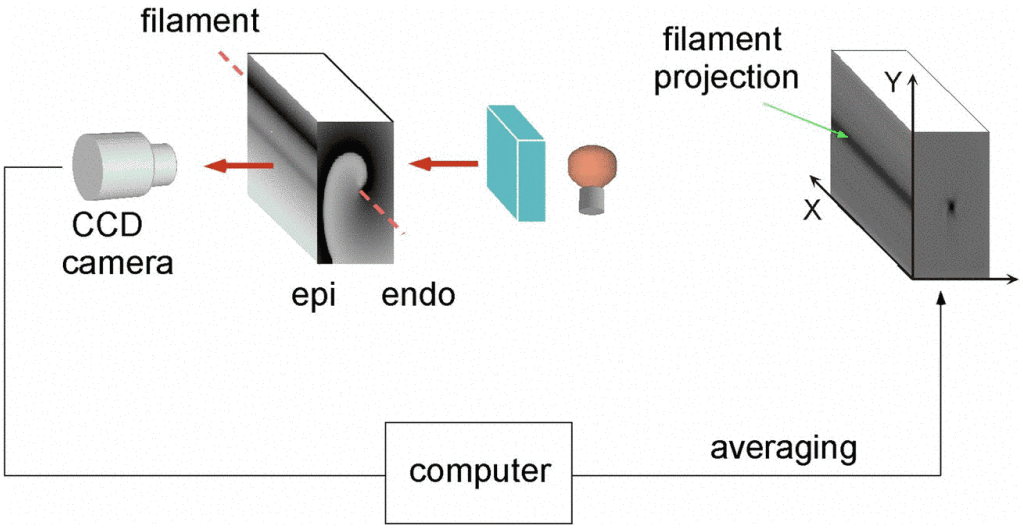

Intramural scroll wave

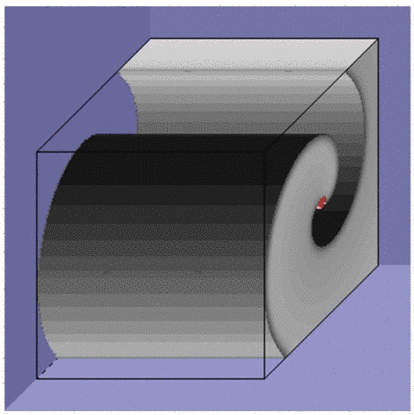

Hybrid model (LRd + optical diffusion)

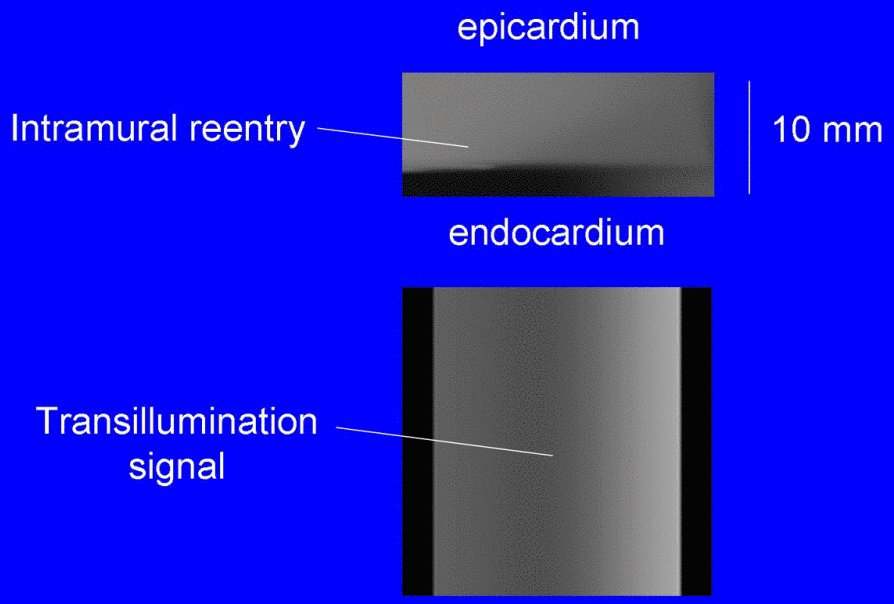

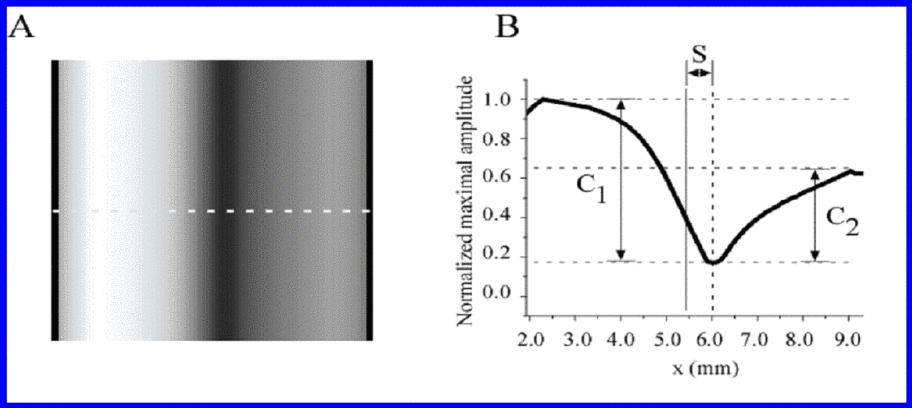

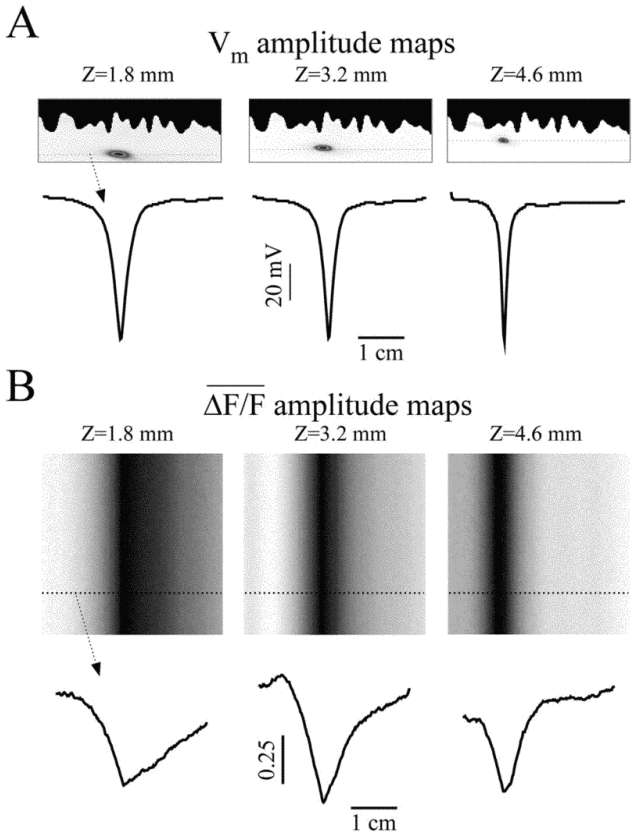

Filament reconstruction (sheep, RH-155 staining)

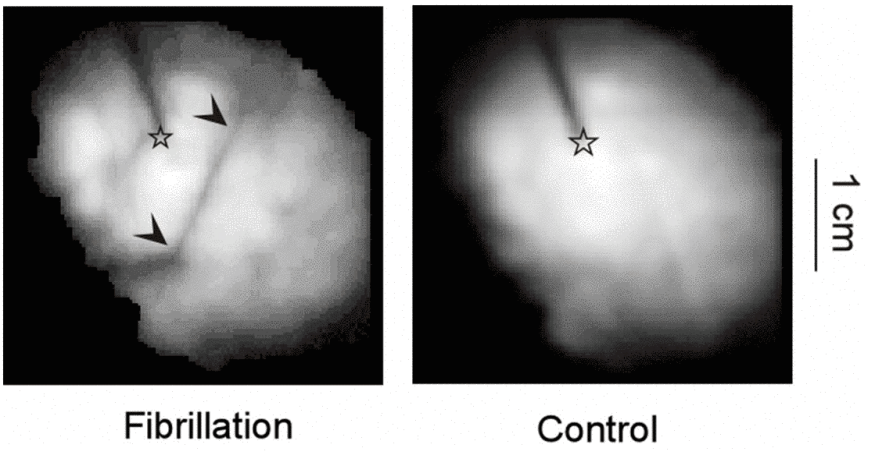

- Filaments tend to stabilize along muscle fibers

(effect is model independent)

Coupling Mediated Alignment

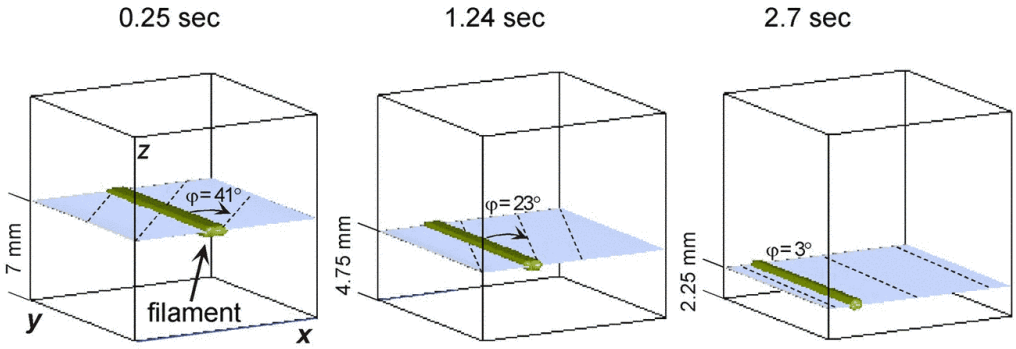

Scroll Wave in Whole Heart Model

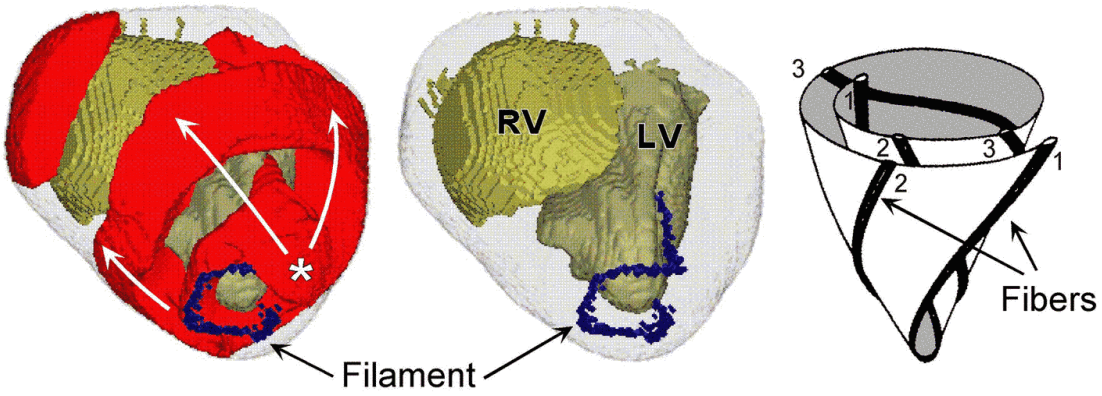

(Berenfeld & Jalife, 1998)

(Torrent-Guasp, 1973)

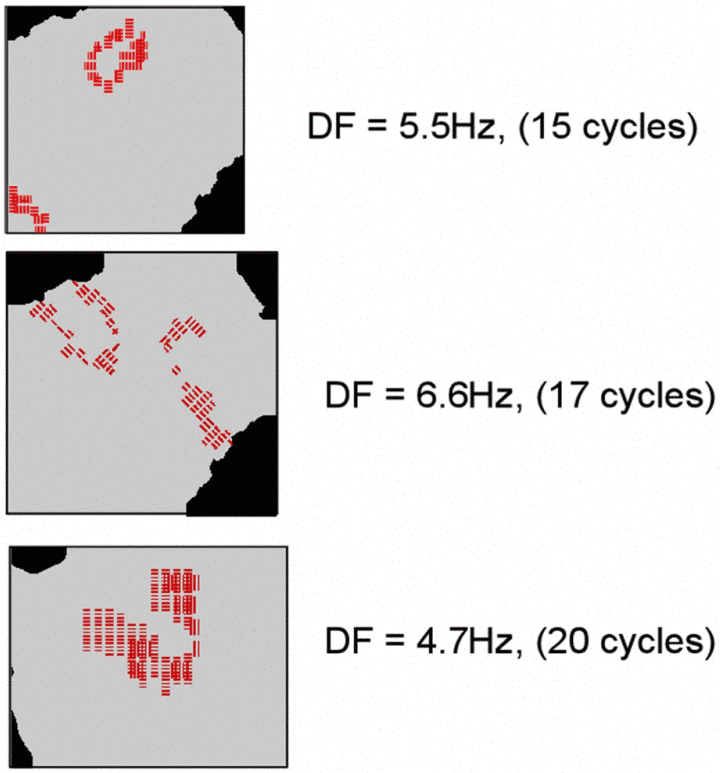

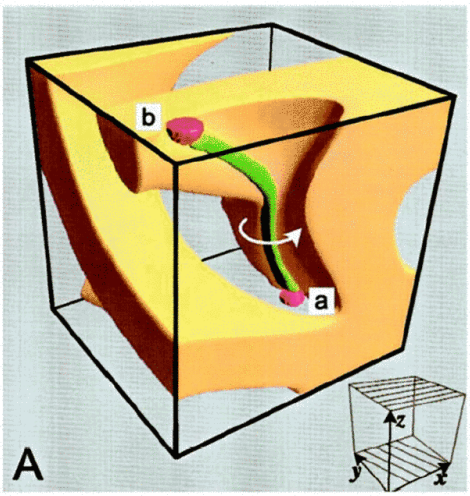

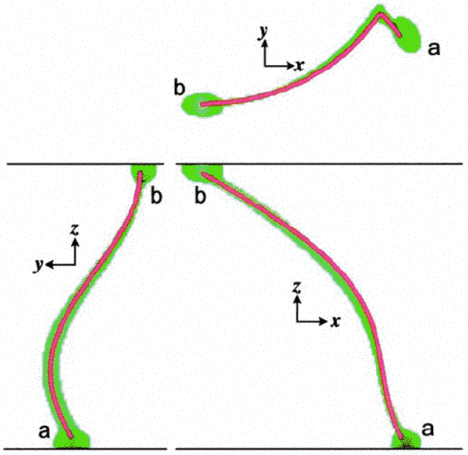

Fig. 2. Comparison between simulation and theory. We present the three orthogonal projections of both the filament (green) and the local geodesic

Paraxial Scanning

extracting depth information

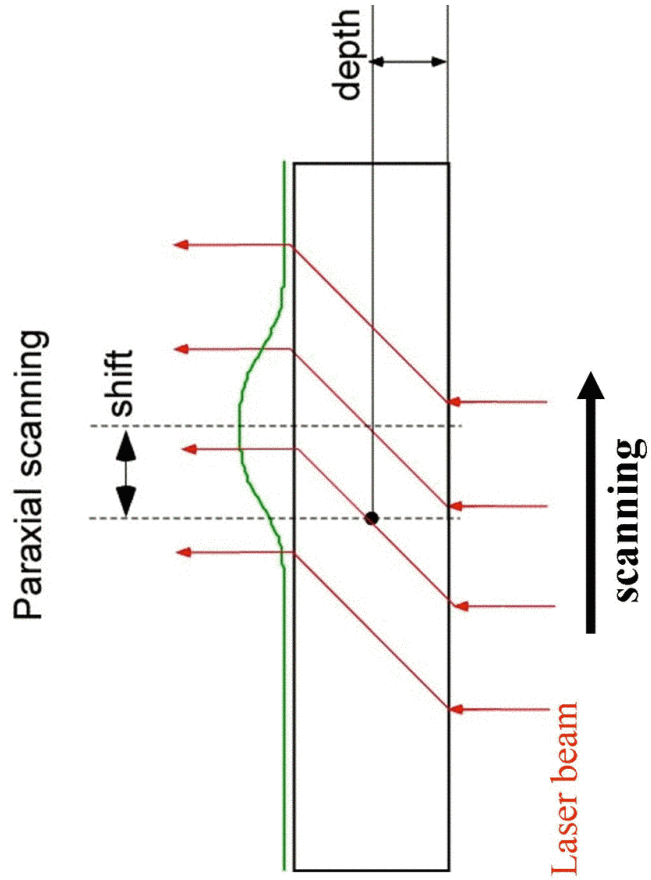
Paraxial scanning
shift
depth
scanning
Laser beam

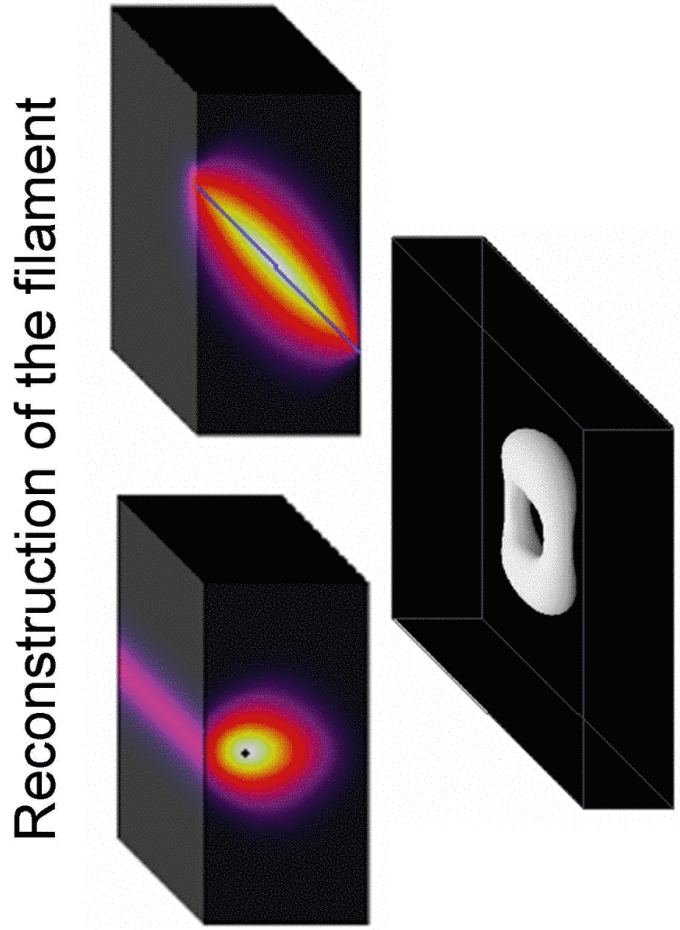
Reconstruction of the filament

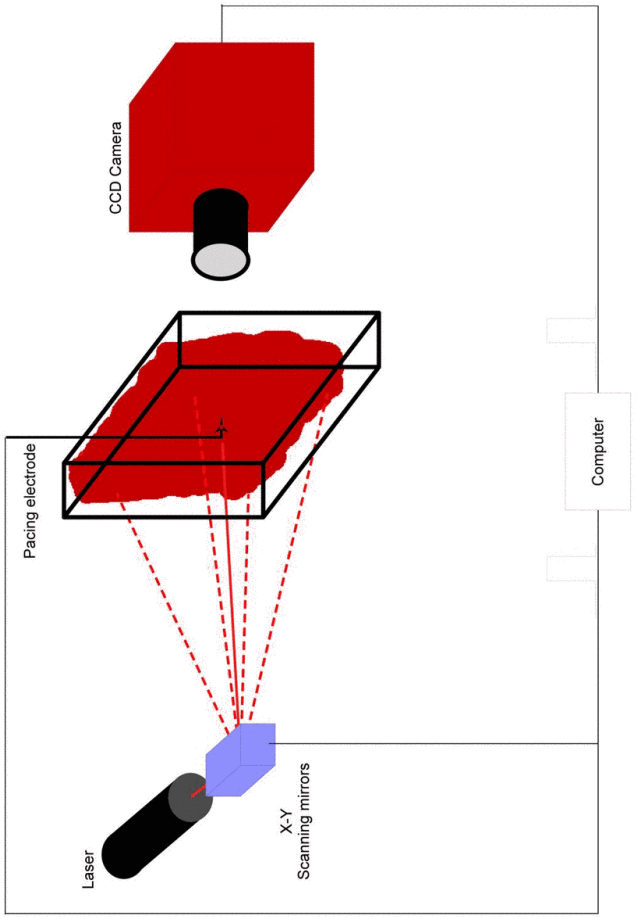

Phantom experiments

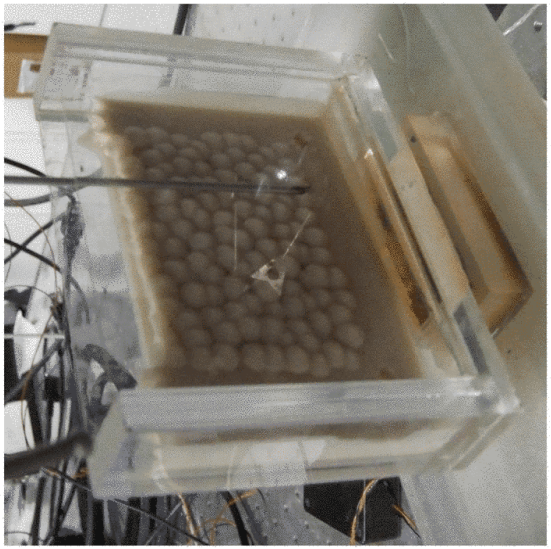

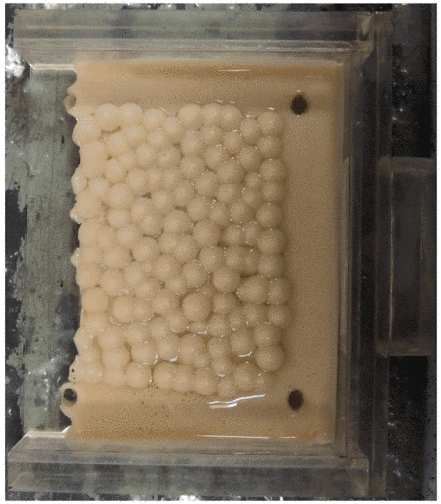

Reconstruction

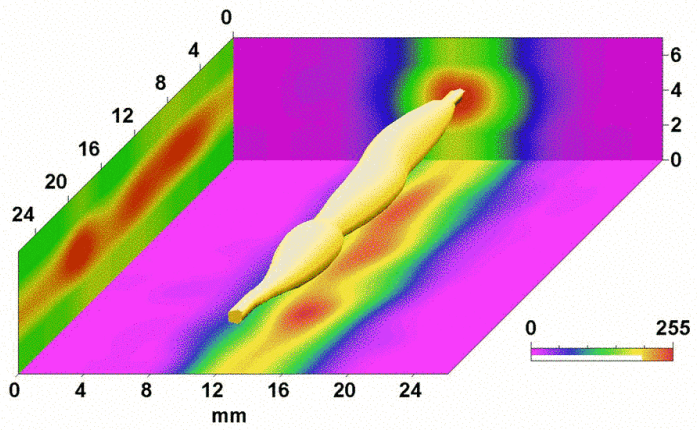

- Scanned area: 40x40 mm
- Reconstructed area: 26x26 mm
- No of points:169
- Object diameter: 2 mm

Porcine RV wall, epicardial pacing(BCL = 300 ms) stained with JPW-5034

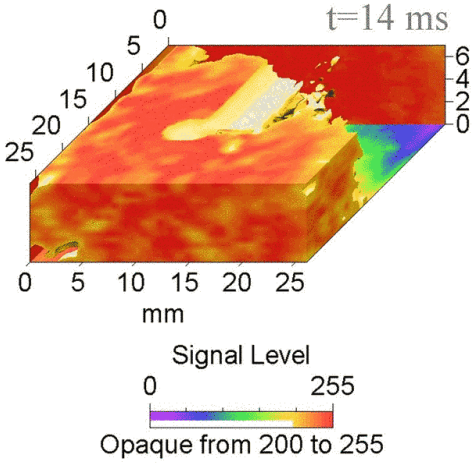

Alternating transillumination

imaging of non-stationary propagation

The idea of the method

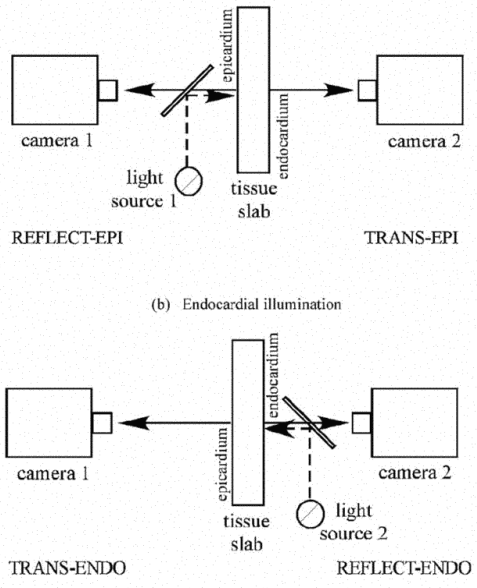

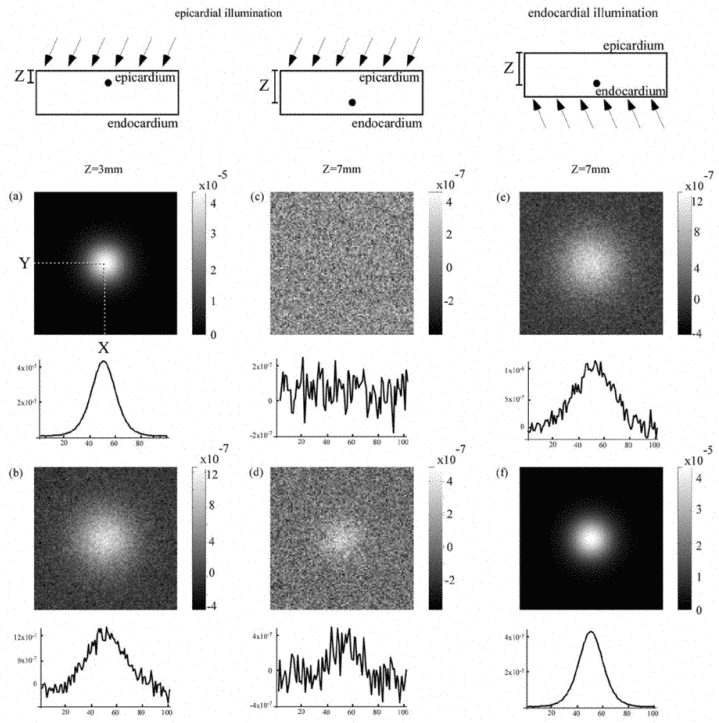

Estimation of depth from integral reflection and transillumination signals

$$Z = \frac{1}{2}\left[L - \delta \ln\left(\frac{J^{\text{refl}}}{J^{\text{trans}}} \right) \right].$$

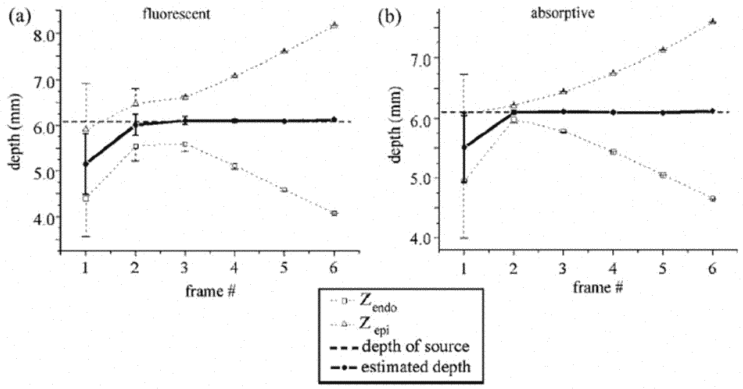

Fig. 5 Accuracy of localizing the excitation center of the expanding hollow ellipsoidal wave using the method of total signal ratios. The actual position of the excitation center (6 mm) is indicated by a dashed line, dotted lines show the calculated depths Z_{epi} and Z_{endo}, and the solid line shows the calculated position of the excitation center. The SD due to noise is indicated for each data point. (a) and (b) are for fluorescence and absorption imaging, respectively.

Quadruplets of images produced by an ellipsoidal front

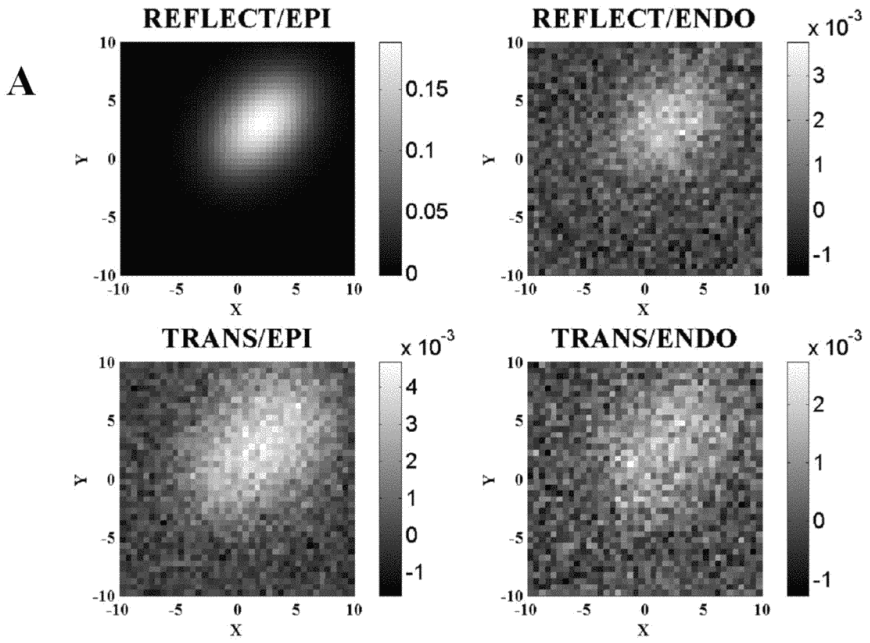

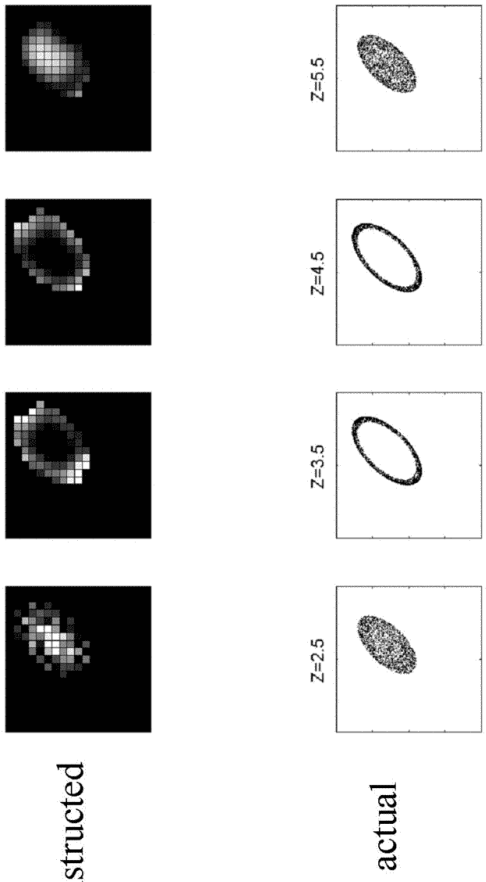
reconstructed
actual
Z=2.5
Z=3.5
Z=4.5
Z=5.5

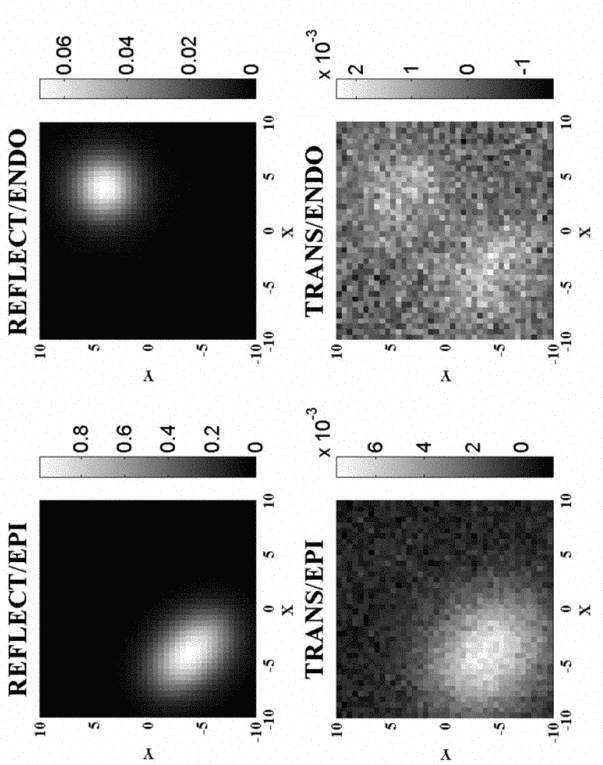
REFLECT/EPI
REFLECT/ENDO
TRANS/EPI
TRANS/ENDO
X
Y

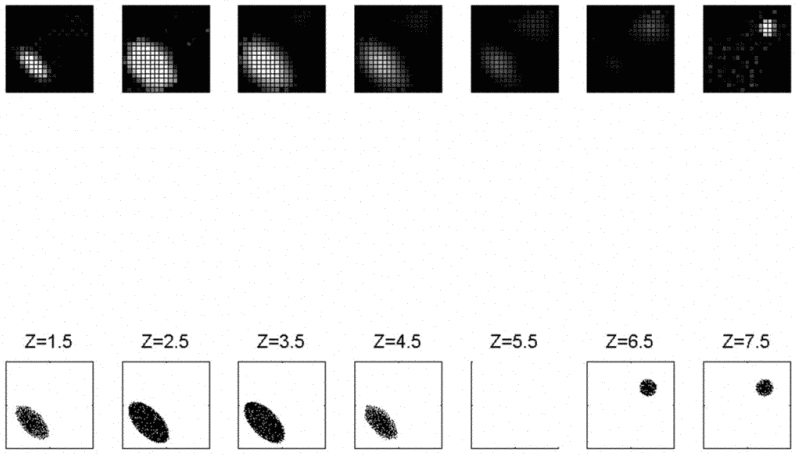

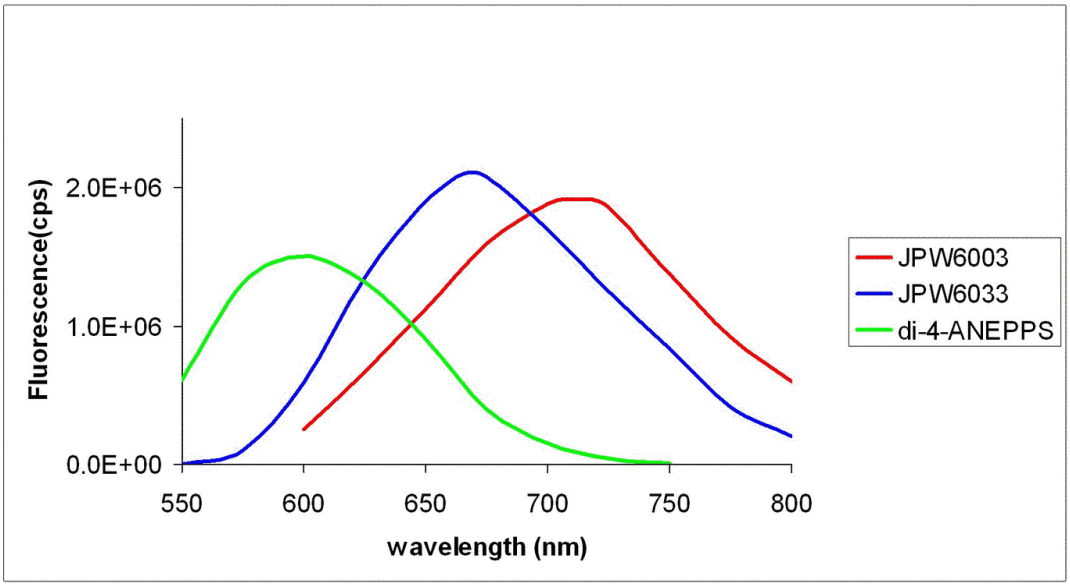

Figure 1. Dye emission spectra in multilamellar lipid vesicles (spectrum of di-4-ANEPPS shown for comparison)

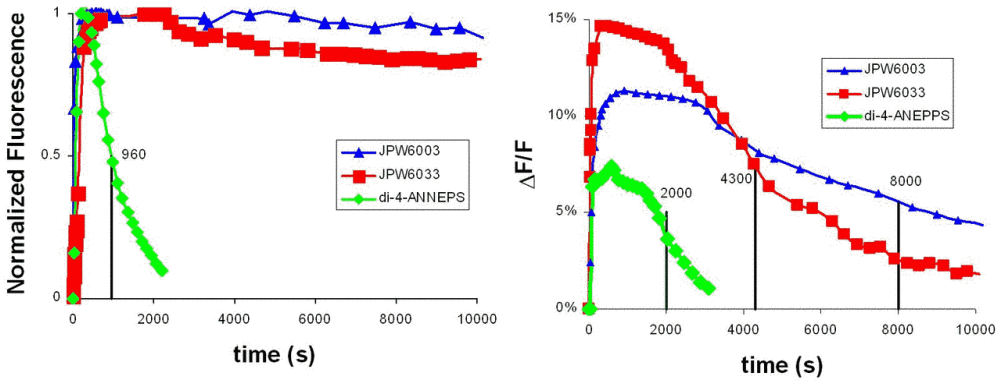

Figure 2. Dye loading and washout dynamics in rat in terms of total (left panel) and voltage-sensitive fluorescence (right panel). Pluronic F-127 was used to load the dye JPW6003 only. Vertical lines show washout half-time.

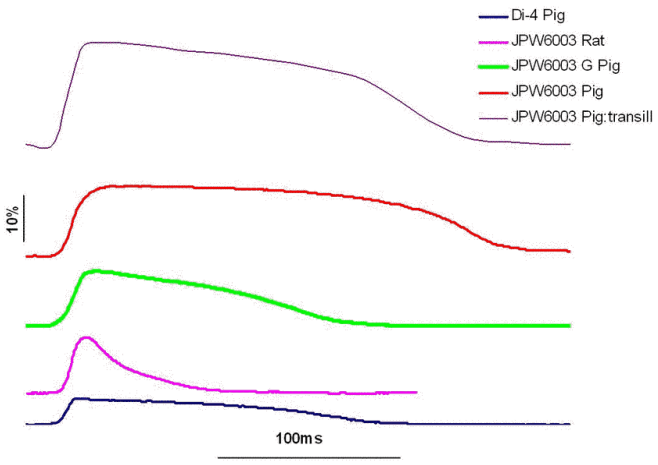

Figure 3. Fluorescence response of the new styryl dye JPW6003 in various cardiac tissues.. Traces from bottom to top correspond to di-4-ANEPPS in pig, and JPW6003 in rat, guinea pig, and pig (epifluorescence and transillumination) respectively.

washout dynamics in pig.

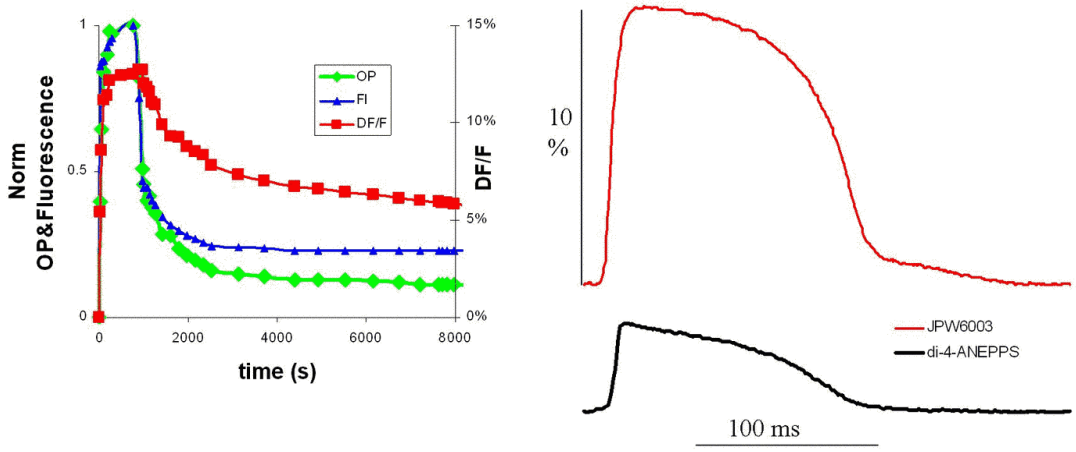

Figure 4. JPW6003 performance in blood perfused pig heart. Left panel shows dye loading and washout dynamics in terms of optical action potential amplitude, total and voltage-sensitive fluorescence. Right panel compares optical potential between JPW6003 and di-4-ANEPPS.

Acknowledgements:

- Christopher Hyatt
- Sergey Mironov
- Fred Vetter
- Marcel Wellner
- Vadim Khait
- Olivier Bernus
- Bogdan Mitrea
- Arvydas Matiukas
- Fred Vetter
- Leslie Loew
- Alexey Zaitsev
- Christian Zemlin